Spin Wave Diffraction and Perfect Imaging of a Grating

S. Mansfeld, J. Topp, K. Martens, J. N. Toedt, W. Hansen, D. Heitmann, and S. Mendach*

Institut für Angewandte Physik und Mikrostrukturforschungszentrum, Universität Hamburg, Jungiusstrasse 11, D-20355 Hamburg, Germany

(Received 15 August 2011; published 26 January 2012)

We study the diffraction of Damon-Eshbach-type spin waves incident on a one-dimensional grating realized by microslits in a thin Permalloy film. By means of time-resolved scanning Kerr microscopy, we observe unique diffraction patterns behind the grating which exhibit replications of the spin wave field at the slits. We show that these spin wave images, with details finer than the wavelength of the incident Damon-Eshbach spin wavelength, arise from the strongly anisotropic spin wave dispersion.

DOI: 10.1103/PhysRevLett.108.047204 PACS numbers: 75.30.Ds, 42.30.Lr, 76.50.+g, 81.05.Xj

The possibility to use spin waves to excite, store, and retrieve electric signals and to perform logical operations relies on the ability to manipulate spin wave propagation. In patterned, thin ferromagnetic films, spin waves with gigahertz frequencies and wavelengths from several hundreds of nanometers up to millimeters can be confined [1–8], focused, and guided [9–14]. An intriguing possibility to guide spin waves in unpatterned films lies in their anisotropic dispersion. The dispersion of dipole-dominated spin waves in thin ferromagnetic films strongly depends on their propagation direction $\vec{k}$ with respect to an in-plane magnetic field $\vec{H}_0$ giving rise to Damon-Eshbach modes with $\vec{k}_{\mathrm{DE}} \perp \vec{H}_0$, backward-volume modes with $\vec{k}_{\mathrm{BV}} \parallel \vec{H}_0$, or a combination of both. This anisotropy in the dispersion of spin waves [15–17] has recently been studied theoretically [18] and experimentally [19–21] as a novel way to manipulate spin wave propagation.

In this Letter, we demonstrate that the anisotropic spin wave dispersion enables perfect imaging with spin waves. We present and discuss time-resolved scanning Kerr microscopy (TR-SKM) [22,23] data on the diffraction of planar Damon-Eshbach spin waves on a one-dimensional grating realized by micrometer-sized slits in a Permalloy film. Behind this grating, we observe a unique diffraction pattern which arises from the interference of Damon-Eshbach and backward-volume-type spin waves and their inherent strongly anisotropic dispersion. We show that this diffraction pattern produces images of the spin wave field at the slits. The resolution of these images is not limited by the wavelength of the incident spin wave, as is the case in isotropic media [24], but deviations from a perfect image occur solely due to spin wave damping and due to the finite curvature of the dispersion's isofrequency line in k space. In that sense, our spin wave images represent a spin wave analogue to subwavelength resolution concepts with anisotropic media in optical metamaterials [25–27]. In both cases, the conditions for perfect imaging, i.e., propagation of all Fourier components and superposition with the correct phase at the image plane, are fulfilled. In addition, we demonstrate that the position of the spin wave images behind the slit array can be tuned by manipulating the spin wave dispersion via the excitation frequency and the external magnetic field. This enables us to create tailor-made spin wave fields in an unpatterned ferromagnet film with submicron resolution.

The experimental arrangement is sketched in Fig. 1. The investigated sample is a 22 nm thick Permalloy film prepared on top of a coplanar wave guide (CPW) structure. The CPW was prepared on a 340 μm thick GaAs(100) substrate and consists of a 3 nm thick adhesive layer of chromium and a 180 nm thick layer of gold. It features a 3 μm wide signal line (S) separated by 2 μm gaps from the ground lines ($G1$ and $G2$). $G2$ exhibits a 150 μm wide gap at the position of the Permalloy film; this guarantees the injection of well-defined planar spin waves from the signal line (S). An approximately 200 nm thick layer of hydrogen silsesquioxane was applied on top of the wave guide, acting as an insulator between the wave guide and

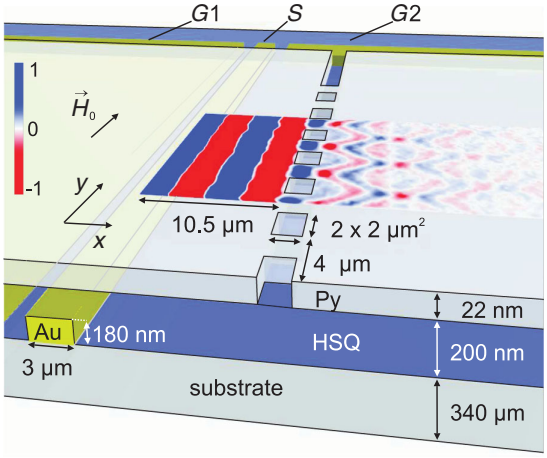

FIG. 1 (color). Sketch of the experimental arrangement. S denotes the signal line, and $G1$ and $G2$ denote the ground lines of the coplanar wave guide. An exemplary TR-SKM phase image of the spin wave field taken at $\mu_0 H_0 = 10$ mT and $f = 4180$ MHz is overlaid as a color density plot on a part of the Permalloy film.

the Permalloy film. The film has a rectangular shape with a length of $l = 280\ \mu$m perpendicular and $w = 120\ \mu$m parallel to the CPW. At a distance of 10.5 μm from the center of the signal line (S), the Permalloy film features a one-dimensional grating realized by 13 square-shaped holes with a side length of 2 μm and a periodicity of $p = 4\ \mu$m. The Permalloy film was prepared using vacuum thermal evaporation in combination with electron beam lithography and lift-off technique.

TR-SKM is used to examine the spin wave propagation in the Permalloy film. A pulsed Titan-Sapphire laser with a wavelength of 800 nm and a repetition rate of 76 MHz is focused onto the sample to probe the magnetization component perpendicular to the Permalloy film via the magneto-optical Kerr effect. The laser focus has a width of approximately 550 nm (as determined by scanning over the CPW's edge) and is scanned over the sample in 250 nm steps. Spin waves are excited in the film by passing a continuous microwave through the CPW. The customized microwave synthesizer (ITS 9200 by MiroSys GmbH and Innovative Technical Systems) used to excite the spin waves is phase-locked to the repetition rate of the laser. By tuning the phase offset between laser and microwave synthesizer, the spin wave field in the sample can be measured phase-dependently. This enables us to image propagating spin wave fields with a temporal resolution of a few picoseconds. Initially, we have optimized the setup shown in Fig. 1 with experiments on homogenous unpatterned films and found that, except for edge effects which extend less than 15 μm from the edges of the film, the CPW emits planar spin waves with wave vectors tunable up to $k = 4.5\ \mu\text{m}^{-1}$. In particular, we do not observe effects of the directly exciting microwave field on the propagating spin wave if we choose the gap structure in the ground line of the CPW to be large enough. The color-encoded plot overlaid onto the sample sketch in Fig. 1 represents an exemplary measurement. As indicated by the arrow, the external magnetic field is oriented parallel to the CPW. All magnetic fields quoted in the following have been applied after applying a saturation field of 130 mT in the y direction and ramping down to 0 mT. A Damon-Eshbach-type spin wave is excited at the signal line (S) and propagates towards the grating. At the grating, the spin wave is partly reflected and partly transmitted. In the following, we investigate the transmitted part and its unique interference patterns. We show that these patterns produce images of the grating at distinct positions.

Let us first concentrate on three TR-SKM images depicted on the left-hand sides of Figs. 2(a), 2(c), and 2(e) and measured at $\mu_0 H_0 = 20$ mT with excitation frequencies of $f_1 = 4180$ MHz, $f_2 = 4636$ MHz, and $f_3 = 5092$ MHz, respectively. (Note that the frequencies used need to be an integer number of the laser repetition rate.) These images show the propagating spin wave field at a defined phase of the excitation; i.e., they represent snapshots of the spin wave field for a certain point in time. In the following, they are referred to as phase plots. The holes in the Py film defining the grating are marked by dashed black lines. For all frequencies, we observe distinct interference patterns which are periodic in the propagation direction (the x direction) and along the grating (the y direction). With increasing frequency, we find that the period in the propagation direction gets smaller while the period along the grating is fixed. This is also reflected in the corresponding spatial Fourier spectra of the areas

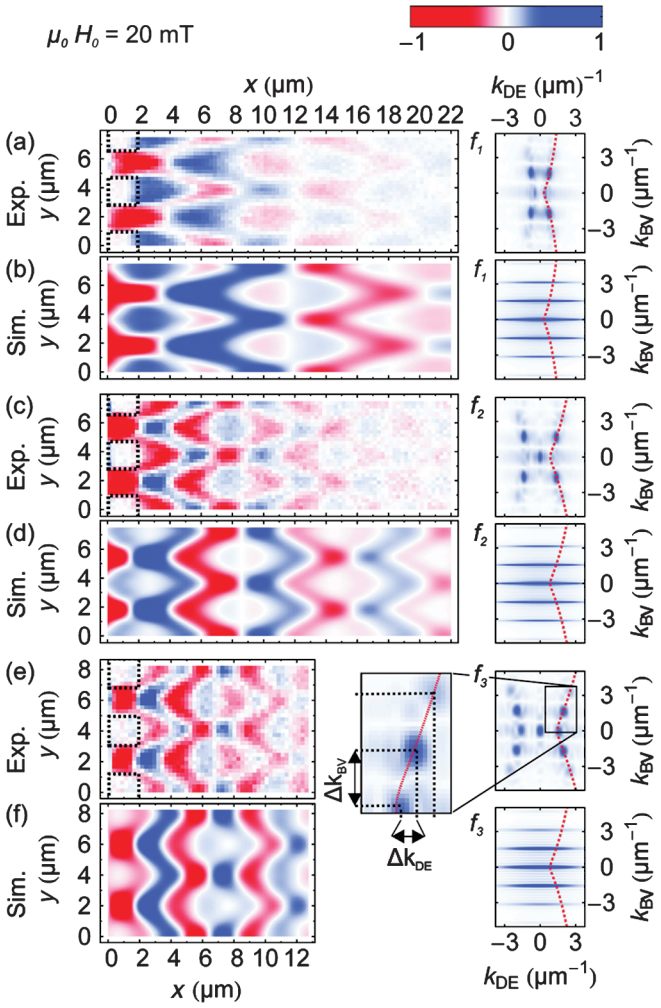

FIG. 2 (color). (a),(c),(e) TR-SKM phase image of the spin wave field (left-hand sides) behind the grating and corresponding Fourier spectra (right-hand sides) measured at $H_0 = 20$ mT, with $f_1 = 4180$ MHz, $f_2 = 4636$ MHz, and $f_3 = 5092$ MHz, respectively. The holes in the Py film defining the grating are marked by dashed black lines in the TR-SKM images on the left-hand sides. (b),(d),(f) Calculated spin wave fields for $f_1 = 4180$ MHz, $f_2 = 4636$ MHz, and $f_3 = 5092$ MHz (left-hand sides) and Fourier spectra of an analytical approximation of the slit array. Here, k_{DE} and k_{BV} are, respectively, spin wave vector components in the x direction and in the y direction. The red dashed lines plotted in all Fourier spectra mark the theoretical DIFL.

behind the gratings, which are shown on the right-hand sides of Figs. 2(a), 2(c), and 2(e). We observe well-defined intensity maxima in the Fourier spectra which correspond to the spin wave modes contributing to the respective interference pattern. Additionally, we find peaks for $k_{DE} = 0$ and $k_{BV} = 0$, which are not related to the propagating spin wave field. The backward-volume components $|k_{BV}|$ of the observed modes correspond to the grating period in the y direction ($p = 4\ \mu$m) and are the same for all excitation frequencies ($|k_{BV0}| = 0$, $|k_{BV1}| = 1.65\ \mu\text{m}^{-1}$, and $|k_{BV2}| = 3.30\ \mu\text{m}^{-1}$). In contrast to this, the related Damon-Eshbach components $|k_{DE}|$ which correspond to the period in the propagation direction increase with increasing frequency. They are imposed by the anisotropic dispersion law of spin waves in the Py film, since only wave vectors fulfilling this dispersion law can propagate away from the grating. Therefore, the experimental Fourier spectra shown in Figs. 2(a), 2(c), and 2(e) give the convolution of the grating's Fourier spectrum with the dispersion's isofrequency line (DIFL) in k space at different frequencies. (The DIFL is also referred to as a "slowness curve" in recent literature [18,21].) Indeed, we find that the observed maxima fit very well with calculated DIFLs (red dashed lines) obtained with an analytical model by Kalinikos *et al.* [28] for a 22 nm thin ferromagnetic film with a saturation magnetization of $\mu_0 M_s = 0.94$ mT.

A first-principles calculation of the diffraction pattern would be an extremely challenging task. It would require a detailed knowledge of the static spin boundary condition at the edges of the holes and the arising static and dynamic magnetization pattern at the grating in an external magnetic field. Micromagnetic simulations of the sample using the OOMMF framework [29] show the same general features as in the measurements. However, we find that, with a simple analytical ansatz, we can reproduce the observed interference patterns in more detail and get a deeper insight into the mechanism which leads to the formation of the patterns: We use an array of 13 intensity distributions $s(\vec{r}) = S_0 \exp(-2\vec{r}^2\ \mu\text{m}^{-2})$ spaced 4 μm apart as an approximation of the spin wave distribution at the grating. The phases and amplitudes of all modes excited by the diffraction are calculated by taking the Fourier spectrum of this intensity distribution. To obtain those modes of the spectrum which can propagate in the Permalloy film, we convolute the Fourier spectrum of the grating with the calculated DIFLs. This is illustrated in the right-hand sides of Figs. 2(b), 2(d), and 2(f). By superimposing all, in this way identified, propagating modes with the correct amplitude and phase in real space, we calculate the spin wave interference patterns shown on the left-hand sides of Figs. 2(b), 2(d), and 2(f). We find a good agreement with the corresponding experimental data shown in Figs. 2(a), 2(c), and 2(e). Small deviations in the details of the spin wave patterns are due to the simple approximation we use for the spin wave distribution at the slit array. To examine the exact spin wave boundary conditions at the slits is an interesting task in itself which we will address in future experimental and theoretical works. Note that it is not sufficient to assume point sources to obtain a good agreement between calculation and experiment.

Figure 3(a) shows an amplitude plot which was measured at $f_2 = 4636$ MHz and $H_{ext} = 20$ mT and corresponds to the phase plot shown in Fig. 2(c). To obtain the amplitude plot, we scanned through a complete phase period and measured the maximum deflection of the magnetization for all spatial points in the measured field. We find distinct areas with high amplitudes (blue color) and areas with amplitudes near zero (white color). The sharp features in the pattern, e.g., the white lines with a small width of approximately 700 nm compared to the incident Damon-Eshbach wavelength of 6.3 μm, indicate the excitation of high k_x and k_y components at the grating.

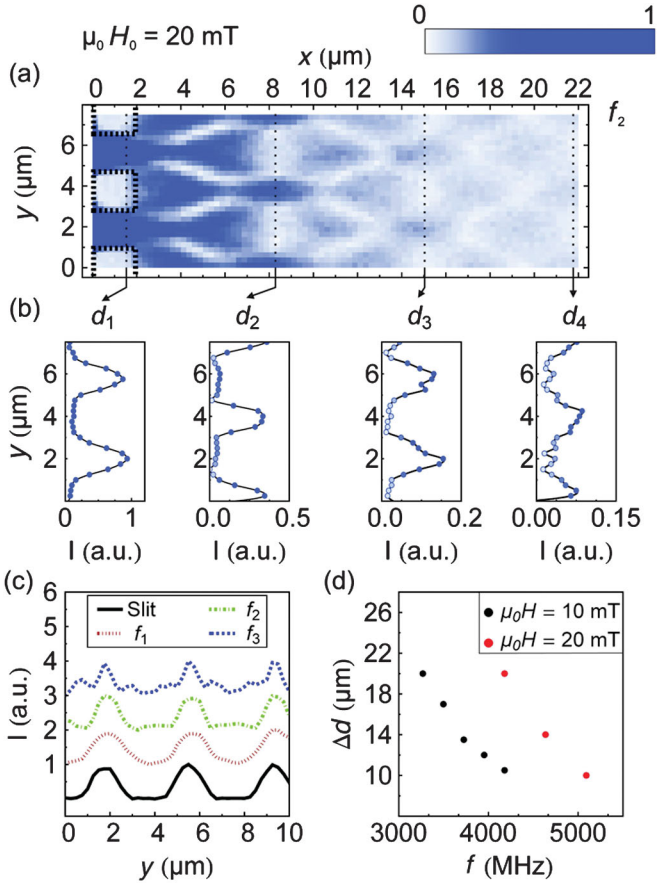

FIG. 3 (color). (a) TR-SKM amplitude image of the spin wave field at $H_0 = 20$ mT and $f_2 = 4636$ MHz corresponding to the left-hand side of Fig. 2(c). The holes in the Py film defining the grating are marked by thick dashed black lines. (b) Cross sections along the thin dashed black lines at d_1, d_2, d_3, and d_4. (c) Cross sections along the first image line measured at $f_1 = 4180$ MHz, $f_2 = 4636$ MHz, and $f_3 = 5092$ MHz. (d) Distance between grating and image line Δd at $\mu_0 H_0 = 10$ mT (black dots) and $\mu_0 H_0 = 20$ mT (red dots).

Most interestingly, the amplitude distribution at the grating ($d_1 = 1.50\ \mu$m) is replicated at equidistant x values $d_2 = 8.25\ \mu$m, $d_3 = 15.00\ \mu$m, and $d_4 = 21.75\ \mu$m, where every other replication is shifted in the y direction by half of the grating period p. Figure 3(b) illustrates the replications at the respective x values. They represent spin wave images of the grating cross section, as will be explained in the following.

In general, to obtain a perfect image of the grating cross section, (i) all Fourier components present at the grating cross section have to reach the respective image lines and (ii) they have to be superimposed with the right phase and with the right weighting of amplitudes. As visible from the Fourier spectra shown on the right-hand sides of Figs. 2(c) and 2(d), condition (i) is fulfilled because the DIFL (dashed red line) crosses all grating diffraction orders which exhibit a considerable intensity; i.e., all Fourier components necessary to obtain an image of the grating cross section can propagate in our film. Condition (ii) is fulfilled due to the almost linear shape of the DIFL in this wave vector regime and frequency regime. Because of this linearity, the spacing between Fourier components in the cross-sectional direction (the y direction), which is given by the reciprocal lattice vector $\Delta k_{\mathrm{BV}} = 2\pi/p$ of the grating, leads to an equidistant spacing of the Fourier components in the propagation direction, with $\Delta k_{\mathrm{DE}} = \gamma \Delta k_{\mathrm{BV}}$ and γ being the slope of the DIFL [cf. with the zoom-in on the Fourier spectrum in Fig. 2(e)]. As a result, beating patterns form in real space, exhibiting image lines at periodic distances $\Delta d = 2\pi/\Delta k_{\mathrm{DE}} = p/\gamma$, at which the phases of all Fourier components correspond to the grating cross section. Furthermore, halfway between these image lines, additional image lines exist, where the phases of all Fourier components are shifted by 180° compared to the grating cross section, leading to an image shift in the y direction by $p/2$. Since the cross section of the spin wave field at all x positions inside the slits is imaged as explained above, we in fact observe two-dimensional images of the slits in Fig. 3(a).

Since the slope γ of the DIFL changes with frequency f [cf. Figs. 2(a), 2(c), and 2(e)] and magnetic field H_0, we can tailor the period of the image lines $\Delta d = p/\gamma$, i.e., their position in the film, via f or H_0. As shown in Fig. 3(d), we find that Δd increases with increasing magnetic field and decreasing frequency. With the parameters of our experiment, we obtain values between 10 μm and 20 μm.

Figure 3(c) compares how the spin wave cross section at d_1 is imaged in the respective image lines for $f_1 = 4180$ MHz, $f_2 = 4636$ MHz, and $f_3 = 5092$ MHz at $\mu_0 H_0 = 20$ mT. While the image quality at f_1 and f_2 is comparable, the shorter spin wave damping length at f_3 leads to a reduction in image quality. In measurements on a 20 nm thick Py film without grating, we found that the $1/e$ amplitude damping length decreases from approximately 17 μm to approximately 5 μm if we increase the excitation frequency from 3800 MHz to 5000 MHz. Besides the spin wave damping, which degrades the quality of the images also with increasing distance from the grating [cf. Figure 3(b)], deviation from a perfect image occurs due to the finite curvature of the DIFL which smears out the x position of the image lines. Note that, as visible at $d_2 = 8.25\ \mu$m in Fig. 3(b), this smearing out can also lead to a reduction of the imaged slit width compared to the slit width in the object at $d_1 = 1.50\ \mu$m.

Aside from the perfect spin wave images presented here, another consequence of the linear DIFL is the formation of caustic spin wave beams with direction given by the normal of the DIFL, as discussed in recent literature [19–21]. While these caustic beams do not appear in the diffraction pattern of our grating structure, we indeed observe caustic beams in a double-slit structure (not shown) which was prepared in accordance to the grating structure. The appearance of caustic beams in the double-slit structure is most probably due to its smoother Fourier spectrum compared to the grating. Interestingly, we found one single slit's spin wave image at the crossing of the caustic beams. This reflects the fact that the crossing points of the caustic beams coincide with the image lines discussed above.

In conclusion, we investigated the diffraction of planar Damon-Eshbach spin waves incident on a grating and on a double slit by means of TR-SKM measurements. We found that, due to the linearly shaped DIFL, spin wave images of the slits form behind the structures. The quality of these images is only limited by spin wave damping and the deviation of the DIFL from a linear shape. Furthermore, we demonstrated that the image position in the film behind the periodic structures can be tuned by changing the slope of the DIFL via the excitation frequency or external magnetic field. These findings enable new concepts for controlled spin wave confinement and manipulation in unpatterned ferromagnetic films via adjacent slit arrays, e.g., to realize novel spin wave filters or logic devices.

We acknowledge major contributions to the setting up of our TR-SKM by Jan Podbielski and Andreas Krohn, as well as fruitful discussions with Andreas Rottler and Stephan Schwaiger and financial support from the DFG via SFB 668, SFB 508, and GrK 1286 and from the City of Hamburg via the Cluster of Excellence Nano-Spintronics.

*smendach@physnet.uni-hamburg.de

[1] J. Jorzick, S. O. Demokritov, C. Mathieu, B. Hillebrands, B. Bartenlian, C. Chappert, F. Rousseaux, and A. N. Slavin, Phys. Rev. B **60**, 15194 (1999).

[2] M. Buess, R. Höllinger, T. Haug, K. Perzlmaier, U. Krey, D. Pescia, M. R. Scheinfein, D. Weiss, and C. H. Back, Phys. Rev. Lett. **93**, 077207 (2004).

[3] C. Bayer, J. Jorzick, B. Hillebrands, S. O. Demokritov, R. Kouba, R. Bozinoski, A. N. Slavin, K. Y. Guslienko, D. V.

Berkov, N. L. Gorn, and M. P. Kostylev, Phys. Rev. B **72**, 064427 (2005).
[4] K. Perzlmaier, M. Buess, C. H. Back, V. E. Demidov, B. Hillebrands, and S. O. Demokritov, Phys. Rev. Lett. **94**, 057202 (2005).
[5] I. Neudecker, K. Perzlmaier, F. Hoffmann, G. Woltersdorf, M. Buess, D. Weiss, and C. H. Back, Phys. Rev. B **73**, 134426 (2006).
[6] J. Podbielski, F. Giesen, and D. Grundler, Phys. Rev. Lett. **96**, 167207 (2006).
[7] S. Mendach, J. Podbielski, J. Topp, W. Hansen, and D. Heitmann, Appl. Phys. Lett. **93**, 262501 (2008).
[8] F. Balhorn, S. Mansfeld, A. Krohn, J. Topp, W. Hansen, D. Heitmann, and S. Mendach, Phys. Rev. Lett. **104**, 037205 (2010).
[9] M. Bauer, C. Mathieu, S. O. Demokritov, B. Hillebrands, P. A. Kolodin, S. Sure, H. Dötsch, V. Grimalsky, Y. Rapoport, and A. N. Slavin, Phys. Rev. B **56**, R8483 (1997).
[10] M. Bauer, O. Büttner, S. O. Demokritov, B. Hillebrands, V. Grimalsky, Y. Rapoport, and A. N. Slavin, Phys. Rev. Lett. **81**, 3769 (1998).
[11] V. E. Demidov, S. O. Demokritov, K. Rott, P. Krzysteczko, and G. Reiss, Appl. Phys. Lett. **91**, 252504 (2007).
[12] J. Topp, J. Podbielski, D. Heitmann, and D. Grundler, Phys. Rev. B **78**, 024431 (2008).
[13] V. E. Demidov, S. O. Demokritov, K. Rott, P. Krzysteczko, and G. Reiss, Phys. Rev. B **77**, 064406 (2008).
[14] V. E. Demidov, J. Jersch, S. O. Demokritov, K. Rott, P. Krzysteczko, and G. Reiss, Phys. Rev. B **79**, 054417 (2009).
[15] O. Büttner, M. Bauer, S. O. Demokritov, B. Hillebrands, Y. S. Kivshar, V. Grimalsky, Y. Rapoport, and A. N. Slavin, Phys. Rev. B **61**, 11 576 (2000).
[16] V. E. Demidov, B. Hillebrands, S. O. Demokritov, M. Laufenberg, and P. P. Freitas, J. Appl. Phys. **97**, 10A717 (2005).
[17] K. Perzlmaier, G. Woltersdorf, and C. H. Back, Phys. Rev. B **77**, 054425 (2008).
[18] V. Veerakumar and R. E. Camley, Phys. Rev. B **74**, 214401 (2006).
[19] V. E. Demidov, S. O. Demokritov, D. Birt, B. O'Gorman, M. Tsoi, and X. Li, Phys. Rev. B **80**, 014429 (2009).
[20] T. Schneider, A. A. Serga, A. V. Chumak, C. W. Sandweg, S. Trudel, S. Wolff, M. P. Kostylev, V. S. Tiberkevich, A. N. Slavin, and B. Hillebrands, Phys. Rev. Lett. **104**, 197203 (2010).
[21] M. P. Kostylev, A. A. Serga, and B. Hillebrands, Phys. Rev. Lett. **106**, 134101 (2011).
[22] M. R. Freeman and J. F. Smyth, J. Appl. Phys. **79**, 5898 (1996).
[23] S. Tamaru, J. A. Bain, R. J. M. van de Veerdonk, T. M. Crawford, M. Covington, and M. H. Kryder, Phys. Rev. B **70**, 104416 (2004).
[24] E. K. Abbe, Arch. Mikrosc. Anat. **9**, 413 (1873).
[25] Z. Liu, H. Lee, Y. Xiong, C. Sun, and X. Zhang, Science **315**, 1686 (2007).
[26] S. Schwaiger, M. Bröll, A. Krohn, A. Stemmann, C. Heyn, Y. Stark, D. Stickler, D. Heitmann, and S. Mendach, Phys. Rev. Lett. **102**, 163903 (2009).
[27] B. Wood, J. B. Pendry, and D. P. Tsai, Phys. Rev. B **74**, 115116 (2006).
[28] B. A. Kalinkos and A. N. Slavin, J. Phys. C **19**, 7013 (1986).
[29] M. J. Donahue and D. G. Porter, National Institute of Standards and Technology Interagency Report No. NISTIR 6376, 1999.